

A RECORD OF THE FINAL PHASE OF GIANT PLANET MIGRATION FOSSILIZED IN THE ASTEROID BELT'S ORBITAL STRUCTURE

MATTHEW S. CLEMENT^{1,2,*}, ALESSANDRO MORBIDELLI², SEAN N. RAYMOND², & NATHAN A. KAIB⁴

MNRAS Letters; accepted

ABSTRACT

The asteroid belt is characterized by an extreme low total mass of material on dynamically excited orbits. The Nice Model explains many peculiar qualities of the solar system, including the belt's excited state, by invoking an orbital instability between the outer planets. However, previous studies of the Nice Model's effect on the belt's structure struggle to reproduce the innermost asteroids' orbital inclination distribution. Here, we show how the final phase of giant planet migration sculpts the asteroid belt, in particular its inclination distribution. As interactions with leftover planetesimals cause Saturn to move away from Jupiter, its rate of orbital precession slows as the two planets' mutual interactions weaken. When the planets approach their modern separation, where Jupiter completes just short of five orbits for every two of Saturn's, Jupiter's eccentric forcing on Saturn strengthens. We use numerical simulations to show that the absence of asteroids with orbits that precess between 24-28 arcsec yr⁻¹ is related to the inclination problem. As Saturn's precession speeds back up, high inclination asteroids are excited on to planet crossing orbits and removed from the inner main belt. Through this process, the asteroid belt's orbital structure is reshaped, leading to markedly improved simulation outcomes.

Keywords: minor planets, asteroids: general, planets and satellites: formation, planets and satellites: dynamical evolution and stability

1. INTRODUCTION

As the giant planets grow within the primordial gas disk, the combination of the Sun's radial force and gravitational torques from the disk and other planets rapidly shepherd them into a mutual resonant configuration (Masset & Snellgrove 2001; Morbidelli & Crida 2007). This scenario is consistent with the number of resonant giant exoplanets discovered (eg: GJ 876 and HR 8799, among others, Mills et al. 2016). After the nebular gas dissipates, the giant planets' orbits continue to evolve via interactions with leftover planetesimals in the primordial Kuiper Belt. Scattering events between these objects and the outermost gas giants preferentially displace material inward, while Jupiter tends to scatter objects out of the system entirely (Fernandez & Ip 1984). These small exchanges of angular momentum cause the giant planets' orbits to diverge, eventually destroying the resonant chain. The Nice Model describes how the global instability induced by this escape from resonance sculpts the primordial solar system into its modern form (Tsiganis et al. 2005; Morbidelli et al. 2005; Gomes et al. 2005; Nesvorný & Morbidelli 2012).

The precise timing of the instability has been the subject of a number of recent studies. A delayed instability would imply a correlation with the late heavy bombardment (a perceived spike in lunar cratering ~ 400 Myr

after gas disk dispersal), the existence of which is now in doubt (Zellner 2017; Morbidelli et al. 2018; Quarles & Kaib 2019). Furthermore, simulations of the Nice Model's effects on the fully formed inner planets routinely over-excite the fragile terrestrial worlds on to orbits where they collide with one another or are lost from the system (Brasser et al. 2013; Kaib & Chambers 2016). The "Jumping Jupiter" (Brasser et al. 2009; Roig et al. 2016) model attempts to resolve this issue by requiring that Jupiter and Saturn's semi-major axes diverge in a step-wise manner towards their modern locations as the result of a close encounter with one of the ice giants. However, studies of the scenario argue for weaker instabilities (Deienno et al. 2018) and large period ratio jumps (Toliou et al. 2016) that are low probability outcomes of statistical studies of the instability (Nesvorný & Morbidelli 2012; Deienno et al. 2017). Furthermore, authors must post-process simulation results by modifying the asteroid belt's initial inclination distribution in order to provide good matches to the modern orbital structure (Roig & Nesvorný 2015; Deienno et al. 2016, 2018). Recent work argued that an early (just a few Myr after gas dissipation) instability (Nesvorný et al. 2018) might fix the terrestrial destabilization problem (Clement et al. 2018, 2019a) without requiring such a specific jump. Such an evolutionary model has the advantage of providing a natural explanation for the disparity between the inferred geological accretion time-scales of Earth ($\gtrsim 50$ Myr; Kleine et al. 2009) and Mars ($\lesssim 5$ Myr; Dauphas & Pourmand 2011). However, Xenon measurements from Comet 67P (Marty et al. 2017) are at odds with an instability occurring before the end of Earth's magma ocean phase. Other successful models (eg: Levison et al. 2015; Izidoro et al. 2015) for terrestrial evolution resolve problems related to Mars' size and formation time by invoking non-uniform disk conditions. In

¹ HL Dodge Department of Physics Astronomy, University of Oklahoma, Norman, OK 73019, USA

² Department of Terrestrial Magnetism, Carnegie Institution for Science, 5241 Broad Branch Road, NW, Washington, DC 20015, USA

³ Observatoire de la Côte d'Azur, BP 4229, 06304 Nice Cedex 4, France

⁴ Laboratoire d'Astrophysique de Bordeaux, Univ. Bordeaux, CNRS, B18N, allé Geoffroy Saint-Hilaire, 33615 Pessac, France

* corresponding author email: matt.clement@ou.edu

particular, the “Grand Tack” model (Walsh et al. 2011; Walsh & Levison 2016) resolves the small Mars problem by arguing that Jupiter migrated into the terrestrial region during the nebular gas phase; thereby truncating the distribution of embryos and planetesimals near Mars’ modern orbit. However, all schemes require a giant planet instability at some time to explain the outer solar system (see recent review in Raymond et al. 2018).

While the Nice Model is successful at explaining most aspects of the solar system’s dynamical state, studies of its consequences in the asteroid belt are all plagued by a common pitfall (O’Brien et al. 2007; Deienno et al. 2016, 2018; Clement et al. 2019b). Specifically, numerical simulations overpopulate the high inclination parameter space in the inner main belt (we define the inner belt as the region of asteroids with semi-major axes less than 2.5 au). In this letter, we examine the dynamical processes responsible for this shortcoming. Additionally, we propose a mechanism through which these high-inclination asteroids are naturally removed that is compatible with any of the various terrestrial evolutionary models.

2. THE ASTEROID BELT INCLINATION PROBLEM

The spatial orientation of orbits in the solar system precess circularly, or rotate, on time-scales much longer than their actual orbital periods. The perturbative effects of these variations within the Keplerian problem (particularly those of the Jupiter-Saturn system) have long been known to drive dynamics in the asteroid belt (Poincare 1892; Morbidelli & Henrard 1991a). In the secular theory of solar system evolution (eg: Milani & Knezevic 1990; Morbidelli & Henrard 1991a; Murray & Dermott 1999), the long-term behavior of the eight planets’ orbital eccentricities (e_i) and longitudes of perihelia (ϖ_i) are described by the solutions to the secular equations of motion:

$$\begin{aligned} e_i \cos \varpi_i &= \sum_j^8 M_{ij} \cos(g_j t + \beta_j) \\ e_i \sin \varpi_i &= \sum_j^8 M_{ij} \sin(g_j t + \beta_j) \end{aligned} \quad (1)$$

The same analysis can be applied to the precession of the planets’ inclination nodes; specifically the behavior of the orbital inclination ($\sin i/2$) and longitude of ascending node (Ω). Secular resonances occur when an object precesses at a rate equal to one of the solar system’s dominant eigenfrequencies. These eigenfrequencies are denoted g_1 - g_8 for the planets’ eccentricity vector precessions, and s_1 - s_8 for the inclination node precessions. The ν_6 resonance is comprised of the orbital semi-major axes and inclinations with precession rates that match the g_6 rate of 28.22 arcsec yr⁻¹, and cuts across the modern asteroid belt (see Fig. 4). There is a clear deficiency of inner belt asteroids with inclinations above the ν_6 resonance and precessions slower than g_6 relative to Nice Model predictions (Morbidelli et al. 2010). In the modern asteroid belt, the ratio of large ($D > 50$ km) asteroids with inclinations above the ν_6 resonance, to those below is ~ 0.08 (referred to in the subsequent text as the ν_6 ratio).

In the current version of the Nice Model, the orbital eccentricities and inclinations of asteroids are excited by secular resonances rapidly moving across the belt region (O’Brien et al. 2007; Deienno et al. 2018). Because simulations of the instability begin with the giant planets in

a more compact configuration, their orbits precess at different rates than they currently do. The locations of their respective secular resonances are displaced as the planets’ orbits change during, and after the instability. Of most importance for the inner asteroid belt, the ν_6 resonance must traverse from ~ 4.5 au to its modern location at ~ 2.05 au, and the ν_{16} (inclination nodes precessing equal to s_6) resonance must sweep from ~ 2.8 au to ~ 1.9 au (Walsh & Morbidelli 2011). The ν_{16} resonance moves inward, and encounters the inner belt first. This process excites inclinations, but leaves the eccentricities of asteroids unaffected. Because of the characteristic shape of ν_6 (Fig. 4), its movement only excites the eccentricities of low-inclination asteroids in the inner belt (often on to planet crossing orbits). Through these processes, many asteroids are stranded on relatively stable, high-inclination, low-eccentricity orbits in the inner main belt (Morbidelli et al. 2010; Clement et al. 2019b).

The fraction of inner main belt asteroids isolated above ν_6 is tied to the smoothness of the giant planets’ migration. Studies of smooth migration utilizing artificial forces substantially deplete the a/i parameter space below ν_6 , and simultaneously overpopulate the high- i region of phase space (Morbidelli et al. 2010; Walsh & Morbidelli 2011). However, lower ν_6 ratios can be achieved with a “Jumping Jupiter” style instability (Brasser et al. 2009; Roig & Nesvorný 2015; Deienno et al. 2016, 2018), or when the full chaos of the event is considered (Clement et al. 2018, 2019b). While many inner belt asteroids’ inclinations are still over-excited in these scenarios, a substantial number survive giant planet migration with inclinations below ν_6 because the important secular resonances do not linger at any particular location (Clement et al. 2018).

3. DEPLETION MECHANISM

Dynamical instabilities are inherently stochastic, and each follows a unique path. When studying the Nice Model, authors typically select systems in which the giant planets’ final orbits are closest to those of the modern solar system (Clement et al. 2018; Deienno et al. 2018). However, this does not guarantee that the simulated planets followed the same evolutionary path as the real ones. As Saturn’s orbit moves away from the Sun following the instability, its precession rate continues to decrease, thereby lowering g_6 to its modern value. Thus the crux of the Nice Model’s ν_6 problem has been in finding a mechanism to deplete asteroids that precess slower than g_6 after the instability strands them above ν_6 . However, these previous studies have neglected the precise effects induced by Jupiter and Saturn’s specific modern configuration. Presently, the solar system’s two most massive planets lie just inwards of a mutual 5:2 mean motion resonance (MMR), with Jupiter completing ~ 4.97 orbits for every two of Saturn’s.

Secular precessions are known to speed-up near MMRs (Milani & Knezevic 1990; Morbidelli & Henrard 1991a). Fig. 1 demonstrates the behavior of the g_6 rate as Jupiter and Saturn approach their modern configuration. Perturbative derivations of the three-body secular Hamiltonian typically expand the problem in Taylor series, and subsequently neglect mass terms of order two or higher (for a full discussion of secular resonances in the asteroid belt see Milani & Knezevic 1990; Morbidelli & Hen-

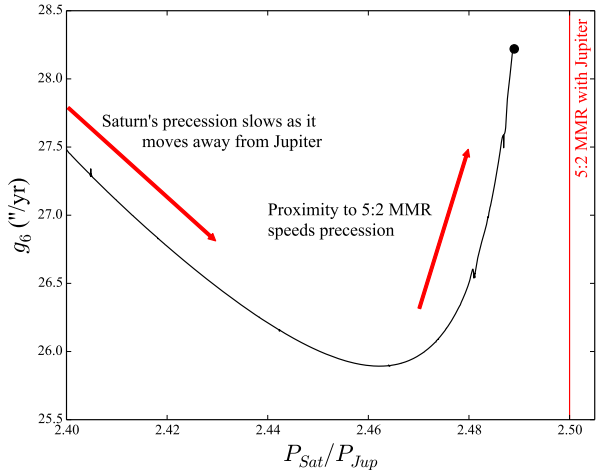


Figure 1. Evolution of the solar system’s g_6 eigenfrequency during Saturn’s final phase of migration. The modern value of g_6 is denoted by a bold point. The figure’s minimum is at $P_{Sat}/P_{Jup} = 2.46$ and $g_6 = 25.89$.

rard 1991a,b). This simplification holds when the bodies’ mean longitudes (λ_i in Delaunay variables) are non-resonant. When the two objects approach a MMR, the quadratic mass term is no longer negligible, and the precession rate g_i increases asymptotically. Our first set of simulations are designed to measure the solar system’s g_6 eigenmode as Jupiter and Saturn approach the 5:2 MMR. We perform 3,200 integrations of the modern solar system with the *Mercury6* hybrid integrator (Chambers 1999). In each run, Saturn’s semi-major axis is decreased by 0.005 au, and all other orbital elements are left unchanged. Each system is integrated for 10 Myr, and the secular amplitudes and frequencies are calculated via Fourier analysis of the simulation time outputs (Šidlichovský & Nesvorný 1996). Through this process, we generate the curve presented in Fig. 1.

As the value of g_6 lowers and rises, the ν_6 resonance shape sweeps from right to left and back in a/i space. We argue that this reversal in sweeping of the ν_6 resonance explains the depletion of asteroids with precession rates less than the current value of g_6 (Figs. 2 and 3) and inclinations above ν_6 in the inner belt region (Fig. 4, top panel).

4. NUMERICAL SIMULATIONS

Next, we use numerical simulations to demonstrate how the reversal of g_6 by just ~ 2.5 arcsec yr^{-1} can affect a uniform population of main belt asteroids about the ν_6 secular resonance (migrating the Jupiter-Saturn period ratio from ~ 2.45 - 2.49). We use the *GENGA* (Grimm & Stadel 2014) integration package for this phase of our study. We first test different migration time-scales by performing three separate simulations of the solar system and 10,000 massless test particles. Asteroid orbital elements are selected randomly from uniform distributions of non-planet-crossing orbits ($2.0 < a < 4.0$ au, $0.0 < e < 0.5$, $0.0 < i < 40.0^\circ$ and 0 - 360° for angular orbital elements). Simply put, the migration is achieved by minor alterations to Saturn’s semi-major axis (by cubic interpolation utilizing *GENGA*’s built in *Set Elements* function) such that the Jupiter-Saturn period ratio evolution follows an exponential function of time un-

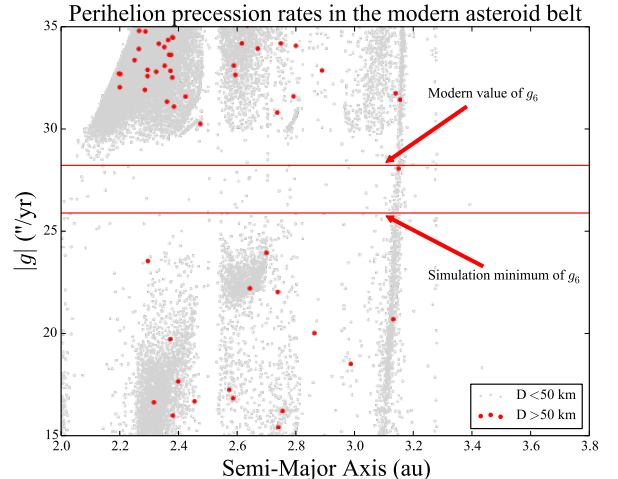


Figure 2. Distribution of orbital precession rates as a function of semi-major axis for all known asteroids with constrained orbits (Knežević & Milani 2003). The horizontal lines represent the current value of Saturn’s g_6 eigenfrequency, and the minimum value obtained from Fig. 1. Red points correspond to large asteroids for comparison with the bottom panel of Fig. 4 (note that the total number of points is less here as this figure is zoomed in on the range of $15 < g < 35$). The asteroids in between the red lines near ~ 3.1 au are members of the high-inclination collisional family (31) Euphrosyne (Novaković et al. 2011). After the break-up of Euphrosyne below the bottom red line, the family members filled the gap that was presumably emptied by primordial migration as the result of semi-major axis spreading due to the Yarkovsky Effect (eg: Bottke et al. 2001).

til reaching the modern value. Each system is integrated for an additional 100 Myr to remove quasi-stable asteroids. Our selected migration speeds (τ_{mig}) are loosely based on studies of Saturn’s smooth migration’s effect on the asteroid belt’s structure (as we seek to study uniform migration after the Nice Model instability; Minton & Malhotra 2011). Specifically, our fastest migration ($\tau_{mig} = 3$ Myr) is selected to equal the slowest sweeping of ν_6 (through the bulk of its migration from 2.8-2.1 au) that permits the asteroid belt’s survival. Because we are only interested in the final phase of migration and clearing in the young solar system, our selected migration speeds are quite slow.

The results of these simulations are summarized in Table 1 and Fig. 3. Through the full migration process, the ν_6 ratio consistently drops from 1.98 to less than unity. Asteroids with high inclinations that would have been unaffected if g_6 had never dipped below ~ 28 arcsec yr^{-1} are quickly swept up and elevated in eccentricity via resonant perturbations (Fig. 3). Once excited, they are eventually removed from the belt as the result of encounters with the terrestrial planets (largely Earth and Mars). Through this process, the inner belt’s overall ν_6 ratio is substantially reduced. Furthermore, these results are independent of the migration time-scale selected (3.0, 10.0 and 30.0 Myr). Since Saturn’s final migration has a strong effect on the inner main belt’s population above the ν_6 resonance regardless of migration speed, we limit τ_{mig} to 5 Myr for the remainder of our study (Morbidelli et al. 2010; Toliou et al. 2016).

As evidenced by the reduction of the ν_6 ratio by a factor of three or so, this mechanism is successful at removing asteroids near ν_6 , but cannot be solely responsible for

Table 1

Initial conditions and results for simulations of a uniform distribution of asteroids: the columns are as follows: (1) the simulation number, (2) the total simulation time, (3) Saturn’s average migration speed for the first 0.04 au, and (4-5) the initial and final ratios of inner main belt ($a < 2.5$ au, $i < 40^\circ$) asteroids above to those below the ν_6 resonance.

Run	τ_{mig}	\dot{r}_{Sat}	ν_6 ratio _i	ν_6 ratio _f
1	3 Myr	0.1 au Myr ⁻¹	1.98	0.81
2	10 Myr	0.03 au Myr ⁻¹	1.98	0.85
3	30 Myr	0.01 au Myr ⁻¹	1.98	0.75

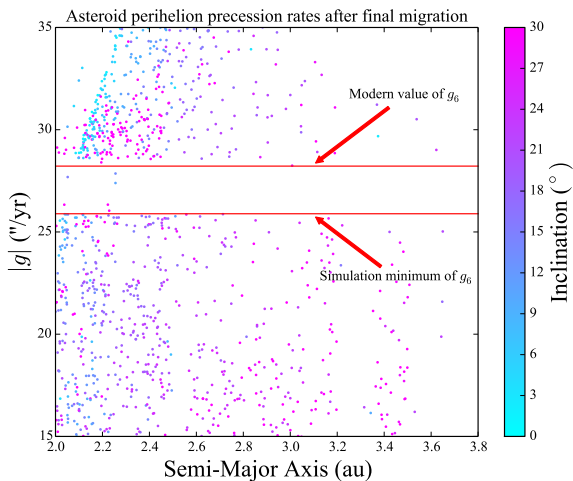


Figure 3. Final asteroid precession rates from our $\tau_{mig} = 30$ Myr simulation of a uniform distribution of asteroids (table 1, run 3). Precession rates are computed by frequency modulated Fourier Transform (see: Šidlichovský & Nesvorný 1996; Knežević & Milani 2003). The colour of each point corresponds to the object’s inclination. Note that, as with Fig. 2, the total number of points here is not 10,000 since many asteroids precess faster or slower than the range of values plotted (particularly in the outer main belt).

generating the modern ratio. Therefore, the ratio must also be limited in Jupiter’s jump phase (Roig & Nesvorný 2015; Deienno et al. 2016; Toliou et al. 2016; Clement et al. 2018; Deienno et al. 2018; Clement et al. 2019b). In our next set of simulations, we investigate asteroid belts formed via terrestrial accretion models (Clement et al. 2018) that experienced a range of jumps. We begin by selecting all surviving asteroids from successful simulations of the Early Instability scenario in Clement et al. (2019b) that finished with $P_{Sat}/P_{Jup} < 2.8$ (using the nomenclature of that work these are runs 1, 3, 6, 1b and 2b). Each system in Clement et al. (2019b) was evolved for 200 Myr, through the Nice Model instability and giant impact phase of terrestrial planet formation. Because a giant planet instability of arbitrary timing is invoked to explain the outer solar system in all terrestrial planet formation models, our initial conditions can be considered roughly independent of evolutionary scheme (Raymond et al. 2018). To improve statistics, we generate 10 separate, 1,000-particle belts by randomly choosing asteroids from these completed simulations, and slightly altering their semi-major axes, eccentricities and inclinations. These small positive and negative deviations are made via random sampling of Rayleigh distributions ($\sigma_a = 0.025$ au, $\sigma_e = 0.025$ and $\sigma_i = 1.0^\circ$). All 8 planets, and the three largest modern asteroids are included for

Table 2

Results for simulations of asteroid belts generated via 200 Myr planet formation simulations (Clement et al. 2019b): the columns are as follows: (1) the simulation number, and (2-3) the initial and final ratios of inner main belt ($a < 2.5$ au, $i < 40^\circ$) asteroids above to those below the ν_6 resonance.

Run	ν_6 ratio _i	ν_6 ratio _f
1	1.45	0.67
2	1.07	0.0
3	1.69	1.14
4	1.37	0.55
5	1.81	0.33
6	2.0	0.25
7	1.12	0.42
8	1.14	1.0
9	1.15	0.60
10	1.63	0.63

these simulations.

We provide the initial and final ν_6 ratios for these simulations in Table 2. The median initial ν_6 ratio for our simulations is ~ 1.4 (as compared to the modern solar system value of ~ 0.08). After 100 Myr of evolution, the overall result of Fig. 3 and Table 1 holds. In the two outlier simulation (runs 3 and 8), the sweeping of ν_6 destabilized many low- i , as well as high- i asteroids. Therefore, while the inclination parameter space above ν_6 was well depleted, the final ratio was still poor.

The inclination structure of a successful simulation (run 5) is plotted in Fig. 4. While the top panel (the post-planet formation belt) broadly matches the concentrations of modern asteroids in different radial bins, the inner main belt is significantly over-populated above the ν_6 resonance. Contrarily, the middle panel (results of this study) is in better overall agreement with the observed belt (final ν_6 ratio of 0.33). From this figure, it is clear that the sweeping most efficiently removes high-inclination objects in the inner main belt. Since all objects with $a \lesssim 2.3$ au have high inclinations initially (the result of the location and movement of ν_{16} , as discussed above), the region’s final a/i structure is altered more dramatically than the $2.3 \lesssim a \lesssim 2.5$ au region.

5. CONCLUSIONS

The Nice Model (Tsiganis et al. 2005; Morbidelli et al. 2005; Gomes et al. 2005; Nesvorný & Morbidelli 2012; Deienno et al. 2017) offers the most consistent explanation for the solar system’s precise dynamical state. Numerous authors have investigated the model’s effect on the asteroid belt’s orbital distribution (Morbidelli et al. 2010; Roig & Nesvorný 2015; Deienno et al. 2016; Clement et al. 2018; Deienno et al. 2018; Clement et al. 2019b). However, previous studies have consistently struggled to match the asteroid belt’s inclination population about the ν_6 resonance. We have shown that this is likely resolved when Jupiter and Saturn’s precise approach to their 5:2 MMR is considered along with the aforementioned works. Our current work, coupled with the well developed Nice Model, thus represents a comprehensive picture of the young solar system’s formation and early evolution.

ACKNOWLEDGEMENTS

This material is based upon research supported by the Chateaubriand Fellowship of the Office for Science and Technology of the Embassy of France in the

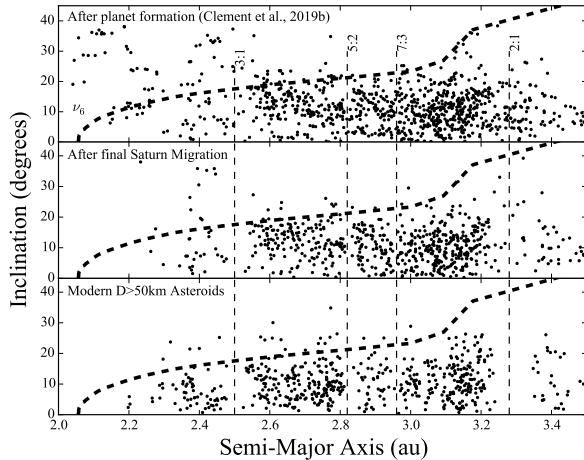


Figure 4. Inclination distribution of our simulated asteroid belt compared with the observed structure. The vertical dashed lines correspond to the semi-major axes of several important mean motion resonances with Jupiter. The bold dashed lines represent the approximate, eccentricity-averaged orientation of the ν_6 secular resonance in a/i space. The top panel depicts the initial conditions for a successful simulation. The middle panel illustrates the same belt’s inclination structure following 5 Myr of Saturn’s final migration inducing a reversal in the sweeping of ν_6 , and 100 Myr of subsequent evolution in the presence of a steady-state solar system. The bottom panel shows the present day asteroid belt’s a/i distribution (only bright objects with absolute magnitude $H < 9.7$, approximately corresponding to $D > 50$ km, are plotted).

United States. M.S.C. and N.A.K. thank the National Science Foundation for support under award AST-1615975. S.N.R. acknowledges NASA Astrobiology Institutes Virtual Planetary Laboratory Lead Team, funded via the NASA Astrobiology Institute under solicitation NNH12ZDA002C and cooperative agreement no. NNA13AA93A. This research is part of the Blue Waters sustained-petascale computing project, which is supported by the National Science Foundation (awards OCI-0725070 and ACI-1238993) and the state of Illinois. Blue Waters is a joint effort of the University of Illinois at Urbana-Champaign and its National Center for Supercomputing Applications.

REFERENCES

- Bottke, W. F., Vokrouhlický, D., Broz, M., Nesvorný, D., & Morbidelli, A. 2001, *Science*, 294, 1693
- Brasser, R., Morbidelli, A., Gomes, R., Tsiganis, K., & Levison, H. F. 2009, *A&A*, 507, 1053
- Brasser, R., Walsh, K. J., & Nesvorný, D. 2013, *MNRAS*, 433, 3417
- Chambers, J. E. 1999, *MNRAS*, 304, 793
- Clement, M. S., Kaib, N. A., Raymond, S. N., Chambers, J. E., & Walsh, K. J. 2019a, *Icarus*, 321, 778
- Clement, M. S., Kaib, N. A., Raymond, S. N., & Walsh, K. J. 2018, *Icarus*, 311, 340
- Clement, M. S., Raymond, S. N., & Kaib, N. A. 2019b, *AJ*, 157, 38
- Dauphas, N., & Pourmand, A. 2011, *Nature*, 473, 489
- Deienno, R., Gomes, R. S., Walsh, K. J., Morbidelli, A., & Nesvorný, D. 2016, *Icarus*, 272, 114
- Deienno, R., Izidoro, A., Morbidelli, A., et al. 2018, *ApJ*, 864, 50
- Deienno, R., Morbidelli, A., Gomes, R. S., & Nesvorný, D. 2017, *AJ*, 153, 153
- Fernandez, J. A., & Ip, W.-H. 1984, *Icarus*, 58, 109
- Gomes, R., Levison, H. F., Tsiganis, K., & Morbidelli, A. 2005, *Nature*, 435, 466
- Grimm, S. L., & Stadel, J. G. 2014, *ApJ*, 796, 23
- Izidoro, A., Raymond, S. N., Morbidelli, A., & Winter, O. C. 2015, *MNRAS*, 453, 3619
- Kaib, N. A., & Chambers, J. E. 2016, *MNRAS*, 455, 3561
- Kleine, T., Touboul, M., Bourdon, B., et al. 2009, *Geochim. Cosmochim. Acta*, 73, 5150
- Knežević, Z., & Milani, A. 2003, *A&A*, 403, 1165
- Levison, H. F., Kretke, K. A., Walsh, K. J., & Bottke, W. F. 2015, *Proceedings of the National Academy of Science*, 112, 14180
- Marty, B., Altwegg, K., Balsiger, H., et al. 2017, *Science*, 356, 1069
- Masset, F., & Snellgrove, M. 2001, *MNRAS*, 320, L55
- Milani, A., & Knezevic, Z. 1990, *Celestial Mechanics and Dynamical Astronomy*, 49, 347
- Mills, S. M., Fabrycky, D. C., Migaszewski, C., et al. 2016, *Nature*, 533, 509
- Minton, D. A., & Malhotra, R. 2011, *ApJ*, 732, 53
- Morbidelli, A., Brasser, R., Gomes, R., Levison, H. F., & Tsiganis, K. 2010, *AJ*, 140, 1391
- Morbidelli, A., & Crida, A. 2007, *Icarus*, 191, 158
- Morbidelli, A., & Henrard, J. 1991a, *Celestial Mechanics and Dynamical Astronomy*, 51, 131
- . 1991b, *Celestial Mechanics and Dynamical Astronomy*, 51, 169
- Morbidelli, A., Levison, H. F., Tsiganis, K., & Gomes, R. 2005, *Nature*, 435, 462
- Morbidelli, A., Nesvorný, D., Laurenz, V., et al. 2018, *Icarus*, 305, 262
- Murray, C. D., & Dermott, S. F. 1999, *Solar system dynamics*
- Nesvorný, D., & Morbidelli, A. 2012, *AJ*, 144, 117
- Nesvorný, D., Vokrouhlický, D., Bottke, W. F., & Levison, H. F. 2018, *Nature Astronomy*, 2, 878
- Novaković, B., Cellino, A., & Knežević, Z. 2011, *Icarus*, 216, 69
- O’Brien, D. P., Morbidelli, A., & Bottke, W. F. 2007, *Icarus*, 191, 434
- Poincare, H. 1892, *Les methodes nouvelles de la mecanique celeste*
- Quarles, B., & Kaib, N. 2019, *AJ*, 157, 67
- Raymond, S. N., Izidoro, A., & Morbidelli, A. 2018, arXiv e-prints, arXiv:1812.01033
- Roig, F., & Nesvorný, D. 2015, *AJ*, 150, 186
- Roig, F., Nesvorný, D., & DeSouza, S. R. 2016, *ApJ*, 820, L30
- Toliou, A., Morbidelli, A., & Tsiganis, K. 2016, *A&A*, 592, A72
- Tsiganis, K., Gomes, R., Morbidelli, A., & Levison, H. F. 2005, *Nature*, 435, 459
- Šidlichovský, M., & Nesvorný, D. 1996, *Celestial Mechanics and Dynamical Astronomy*, 65, 137
- Walsh, K. J., & Levison, H. F. 2016, *AJ*, 152, 68
- Walsh, K. J., & Morbidelli, A. 2011, *A&A*, 526, A126
- Walsh, K. J., Morbidelli, A., Raymond, S. N., O’Brien, D. P., & Mandell, A. M. 2011, *Nature*, 475, 206
- Zellner, N. E. B. 2017, *Origins of Life and Evolution of the Biosphere*, arXiv:1704.06694